Data-driven classification of spectral profiles reveals brain region-specific plasticity

Christina Lubinus[1], Helene Gudi-Mindermann[2], Anne Keitel[3], Andreas K. Engel[4],

Brigitte Röder[2], Johanna M. Rimmele[1,4,*]

Running title: Region-specific spectral plasticity

[1]Department of Neuroscience
Max-Planck-Institute for Empirical Aesthetics
Grüneburgweg 14
D - 60322 Frankfurt am Main, Germany

[2]Biological Psychology and Neuropsychology
University of Hamburg
Von-Melle-Park 11
D - 20146 Hamburg, Germany

[3]Department of Psychology
University of Dundee
Scrymgeour Building
Dundee DD1 4HN

[4]Department of Neurophysiology and Pathophysiology
University Medical Center Hamburg-Eppendorf
Martinistraße 52
D - 20246 Hamburg, Germany

Corresponding author:
Johanna M. Rimmele, PhD
Department of Neuroscience
Max-Planck-Institute for Empirical Aesthetics
Grüneburgweg 14
D - 60322 Frankfurt am Main, Germany
phone: +49 (69) 8300479-323
Email: johanna.rimmele@ae.mpg.de

Abstract

The human brain exhibits rhythms that are characteristic for anatomical areas and presumably involved in diverse perceptual and cognitive processes. Visual deprivation results in behavioral adaptation and cortical reorganization, particularly affecting sensory cortices. Whether these plasticity-related changes are accompanied by altered spectral properties of neural signals and whether certain brain areas are particularly targeted by these changes is unknown. With a recently introduced approach, we analyzed MEG resting state data of a group of congenitally blind and matched sighted individuals. First, using clustering procedures (k-means and Gaussian Mixture Models) we identified brain region-specific spectral clusters. Second, a classifier was employed to test the specificity of the spectral profiles within and the differences between groups. We replicated the previously reported finding of area-specific spectral profiles, indicated by high classification performance in the sighted. Additionally, we found high classification performance in the blind, suggesting that after deprivation-related restructuring, area-specific spectral profiles can be consistently identified. Crucially, in the cross-group classification (sighted vs. blind), several sensory (visual and auditory) and right frontal brain areas were classified significantly worse compared to the control condition. Overall the spectral profiles of those brain areas showed increased neuronal power in higher frequency-bands, possibly reflecting acceleration of the regionally prevalent brain rhythms in the blind compared to the sighted. We provide evidence that visual deprivation-related plasticity selectively alters the spectral profiles of right frontal and sensory brain areas, possibly reflecting increased temporal processing capabilities (auditory, frontal cortices) and changes in the visual inhibitory-excitatory circuits in the blind.

Introduction

The behavioral and neuronal changes associated with visual deprivation-related plasticity offer a unique opportunity to get new insights into the plasticity of intrinsic brain rhythms. In congenital blindness, sensory deprivation is associated with adaptive behavior and neural reorganization. Congenitally blind individuals (CB) were repeatedly reported to show behavioral advantages in a range of different auditory (e.g. pitch discrimination (1), sound localization (2,3), voice recognition (4,5), or temporal order processing (6,7)), tactile (e.g. temporal order processing (6,8)) and higher-level cognitive tasks (e.g. auditory (9) and verbal memory (10,11); temporal attention (12), musical meter perception (13,14), temporal order verbal working memory (15), the perception of ultra-fast speech (16–19)), when compared to normally sighted controls.

These behavioral changes have been related to observations from neuroimaging studies, which revealed altered structural and functional cortical properties. In particular, the occipital cortex is characterized by decreased surface and volume of primary and association areas related to volumetric atrophies (20,21) but also by increased thickness, possibly related to complex developmental and compensatory plasticity (22,23) in congenital blindness. As has been shown repeatedly, visual areas are recruited during various non-visual tasks which has been referred to as cross-modal plasticity (15,24–28). Visual deprivation-related cortical plasticity, however, is not restricted to the visual system as cortical reorganization has also been observed in the intact, that is auditory (29) and somatosensory (30), cortices, so called intramodal plasticity (31). Additionally, fMRI research revealed altered functional interactions of visual cortex with other cortical areas (26,32–36).

Whether the observed behavioral and neuronal changes in congenital blindness are accompanied by changes in the spectral properties of brain areas, is largely unknown. Brain rhythms have been ubiquitously observed across the cortex (37–39), and specific spectral profiles were associated with anatomical areas (40,41). Brain rhythms most likely reflect the synchronization (phase-alignment) of oscillatory activity across neuronal populations, subserving the formation of both local assemblies and large-scale functional networks (42,43) through dynamical linking of brain areas into coherent functional networks for complex tasks (43–45). Various perceptual, cognitive and motor

3

tasks have been shown to recruit brain rhythms in a task-specific manner (42,46–53). Previous research suggests that ongoing activity recorded during resting state measurements to some extend reflects brain rhythms recruited during tasks-specific performances (40,44,54–56). Thus, resting state measurements have been used to study the intrinsic brain rhythms of brain areas and relate them to functional roles of these areas (in fMRI (57), MEG, EEG (40,41,45,58)).

In congenitally blind individuals, the observation of a reduced or absent visual alpha rhythm is well-established (59–63). Only a few studies, however, have investigated the spectral power of brain areas and functional networks in the CB beyond alpha oscillations and beyond the visual cortex. One such study, investigating resting state MEG, found increased connectivity in the delta and gamma ranges within visual cortex in the CB (62). Interestingly, despite the reduction in visual alpha power, the alpha connectivity between visual cortex and other cortical areas was preserved (Note, however, that the alpha band in this study was defined as a broader frequency band including traditional alpha- and beta-bands, 8-20 Hz). In a sound categorization task, the auditory and visual areas were more strongly connected in the blind, as measured by correlations of gamma band power (64), providing support for the notion of the visual cortex being incorporated into the intact sensory systems carrying out non-visual tasks. Furthermore, recent studies observed increases in beta-band connectivity involving visual cortex in the CB (15,28). Taken together, these results support the hypothesis that spectral properties are subject to plastic changes due to sensory deprivation, whereas the systematics of these changes is unknown (i.e., which brain areas and which spectral bands are affected).

Here, we employed and extended a novel analysis pipeline (Fig 1), introduced by (40), to disclose differences in brain rhythms across spectral frequencies and cortical brain areas between CB and S. We hypothesized that (1) spectral profiles ought to be region-specific and homogenous within the sighted group, enabling the classification of brain regions based on the spectral profiles. (2) Whether the spectral profiles in the congenitally blind are consistently altered by plasticity, and thus would enable the identification of brain regions based on their spectral profiles, was unknown. (3) Visual deprivation-related plasticity was predicted to result in altered spectral profiles, particularly of those brain regions where visual deprivation-related reorganization has been previously

4

shown, such as the sensory cortices. Due to altered spectral properties, classification performance for these regions was expected to drop in a cross-group classification. Our analysis pipeline was capable to overcome limitations of standard analyses of brain rhythms, such as facing a predominant activity of frequencies in the alpha and super-low frequency ranges (1/f) and performing poorly at capturing the brains' temporal dynamics over the course of the recording session (43,58). The pipeline disentangled spectral properties in the lower frequency ranges using segment-based clustering (of source-localized Fourier spectra) on a log-logarithmic frequency scale. The temporal dynamics of the spectral properties were captured by computing clusters across temporal segments of the signal and thus taking the time course of activity into account. The pipeline further comprised a classifier analysis, which aimed to identify brain regions by their own spectral profile, thereby testing the specificity of region-specific spectral fingerprints.

Results

All analyses were carried out for three experimental groups: First, in order to replicate that spectral profiles are brain region-specific, a sighted group, instructed to maintain eyes open and fixate their gaze during the recording (S-EO; N=23), was tested. Second, to test whether spectral profiles were also homogenous within the congenitally blind and, crucially, whether there were differences in the spectral profiles between sighted and blind, the data of blindfolded sighted (S-EC; N=24) and congenitally blind individuals (CB; N=26) were analyzed. Following the pipeline proposed by (40), the following analysis was implemented (for an overview see Fig 1; details in the methods section): Fourier spectra were calculated for the preprocessed and segmented (0.8 s long trials) resting state MEG data, projected into source space and spectrally normalized. To localize region-specific spectral clusters, the brain was parcellated into individual regions (N=115) according to the AAL atlas (65). Single-subject and group-level clustering was applied (k-means (66) and Gaussian Mixture Modelling, GMM (67)), resulting in spectral clusters coherent across subjects per ROI that reflect group-level neural activity in a given brain area. Specificity of the spectral fingerprints of a brain area was assessed by a classifier approach, identifying single-subject anatomical regions (of one half of the group) by their spectral clusters based on group-level clusters

5

from the other half of the group. To this end, first, an experimental group (e.g., the S-EO) was split into a training and a test set. Second, region-specific spectral clusters were calculated for the subjects in the training group. Third, the similarity between the calculated group-level clusters and individual 1st level clusters (test set) was assessed by computing the probability (negative log-likelihood) of the test data given the training model. Thus, we obtained a fit between each individual anatomical region and all 115 brain areas (expressed in probabilities), which were ranked yielding ranks from 1 (best predictor region) to 115 (worst predictor region). This fitting procedure was repeated 1000 times. For the comparison of the sighted and congenitally blind individuals (cross-group condition), the sighted were assigned to the training group, while the test set was formed by the group of congenitally blind participants.
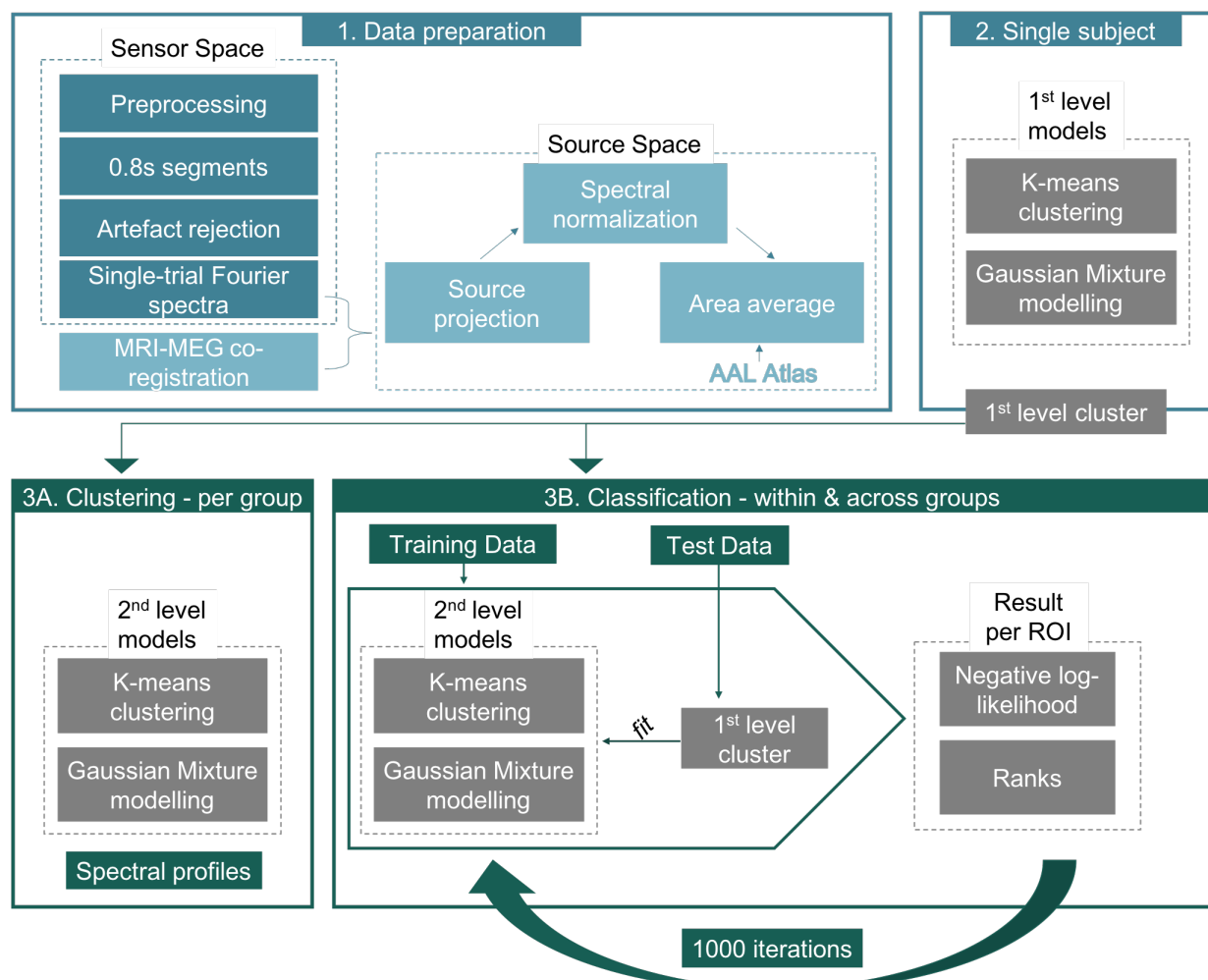

Fig 1. Analysis pipeline (adapted from (40)). (1) Continuous resting state MEG data were preprocessed following general procedures and segmented into trials of 0.8 s length. Complex Fourier spectra were computed for each trial separately and projected into source space using previously defined beam-forming (LCVM) coefficients. The data was spatially normalized, dividing each voxel's power by the mean power of all trials and voxels. Voxels were grouped according to the AAL atlas and power values

were averaged across voxels of each anatomical area (N=115). (2) In the 1st level analysis, power matrices were clustered into 9 distinct spectral clusters per participant and brain region using k-means and Gaussian Mixture model algorithms. (3A) In the 2nd level analysis, 1st level clusters were again subjected to k-means clustering and GGMs to establish region-specific group-level spectral clusters, also referred to as spectral fingerprints in the following. The optimal number of clusters per anatomical area were defined by the Silhouette Criterion prior to the clustering procedure. (3B) For the classification procedure the experimental group was divided into training and test set. For each brain region, the fit between 1st level clusters of the test group and group-level clusters of all regions of the training set was calculated. This resulted in 115 negative log-likelihood values per anatomical region (its similarity to all brain regions (including itself) based on the spectral clusters). This fitting procedure between training and test set was repeated 1000 times with new group assignment (training vs test) on each iteration. To control for inter-individual variance within test and training group, on each iteration, the fitting was repeated 100 times newly drawing a subset from the training and test group (without changing group-assignment).

Spectral fingerprints replicate

In the present study, in our sample of the sighted with open eyes we successfully replicated the classification of individual brain regions by their spectral profiles as first reported by (40). Particularly, the mean classification performance, indicated by the classification ranks, was high (as reported in the Keitel and Gross, 2016 study) (Fig 2). Classification ranks refer to the probability of a region to be identified by the classifier: a rank of 1 implies a region was correctly assigned on every iteration, a rank of 2 implies correct assignment occurred on a majority of the iterations and so forth. Here, the mean rank (averaged across all iterations and brain areas) obtained from the classifier analysis was 2.70 (range of ranks: 1 – 12.7, Keitel mean rank = 1.8), or 2.32 when considering identification of the homologue (left/right hemisphere) areas as a hit (Keitel homologue mean rank=1.4). Mean ranks of all anatomical regions are depicted in the histogram and surface plot in Fig 2. Importantly, we here statistically quantified the classification performance using permutation tests. The mean classification rank of an area (e.g., right calcarine) was tested against a distribution of classification of all brain areas (except the current one, e.g., right calcarine) accumulated across all iterations (N=1000). For an area with a characteristic spectral profile, classification between corresponding areas (e.g., right calcarine in training vs test set) should be best and, thus, fall above the 95th percentile of the generated null-distribution. This analysis revealed that for 97% of all areas classification was significantly better when identifying themselves compared to all other regions.
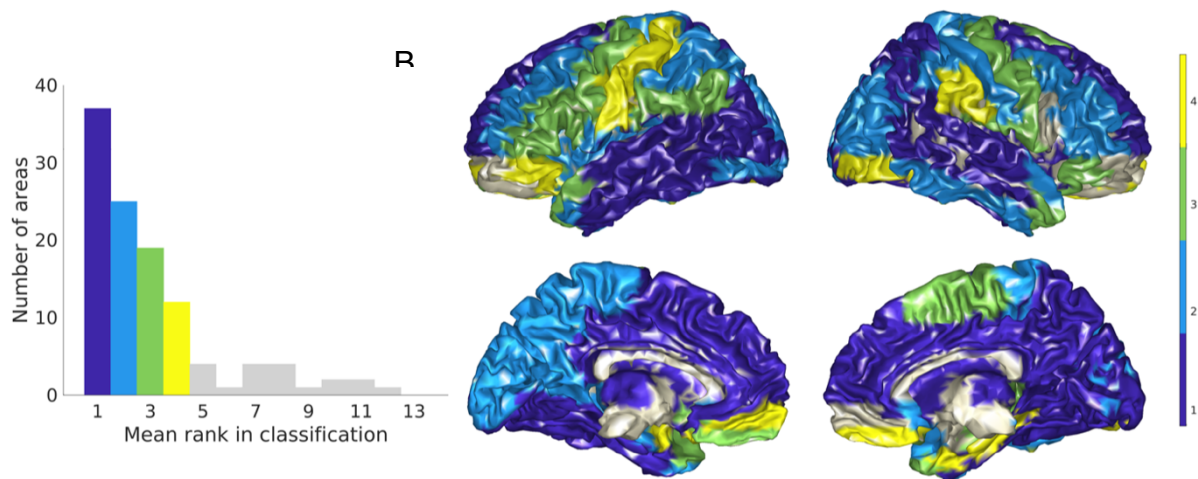
Fig 2. Classification results for the sighted with open eyes (replication sample). (A) Histogram of mean ranks in classification across all 115 brain regions. 84.5% of the brain regions fall within rank 1 to 4, which was the highest rank obtained by Keitel and Gross (2016), while 15.5% of regions were as-signed ranks up to 13. (B) Topography of mean ranks (colors match ranks from the histogram).

Furthermore – although the average optimal number of clusters per anatomical area was lower in our sample (3.4 +- 2.3 clusters per area vs 4.1 +- 1.86 (M + STD) in Keitel & Gross 2016) – the clustering approach revealed comparable spectral fingerprints (see Fig 5). Interestingly, for deeper brain structures the clusters were less character-istic (i.e. only few clusters per area with less specific shapes and high classification ranks) – possibly reflecting limitations of the signal-to-noise-ratio of the used MEG sys-tem (see S1 Fig).

Good classification within sighted and congenitally blind

In order to investigate the spectral differences between the CB and the S (both blind-folded), first, we performed the classification procedure for each group individually to ensure good within group classification (see Fig 3). In both groups, we observed good classification ranks (similar to the ones observed for the S with open eyes) (S-EC: mean rank = 2.64, range = 1-11.4, homologue mean rank = 2.17, percent significant ROIs = 98%; CB: mean rank = 2.51, range = 1 - 10.3, homologue mean rank = 2.10, percent significant ROIs = 100%), indicating consistent spectral clusters of brain areas within groups. This was an important prerequisite for further between-group analyses

because it reassured that potential group differences did not arise from large within group variance. Furthermore, the results showed a similar distribution of mean ranks across the cortical surface for both CB and S-EC.
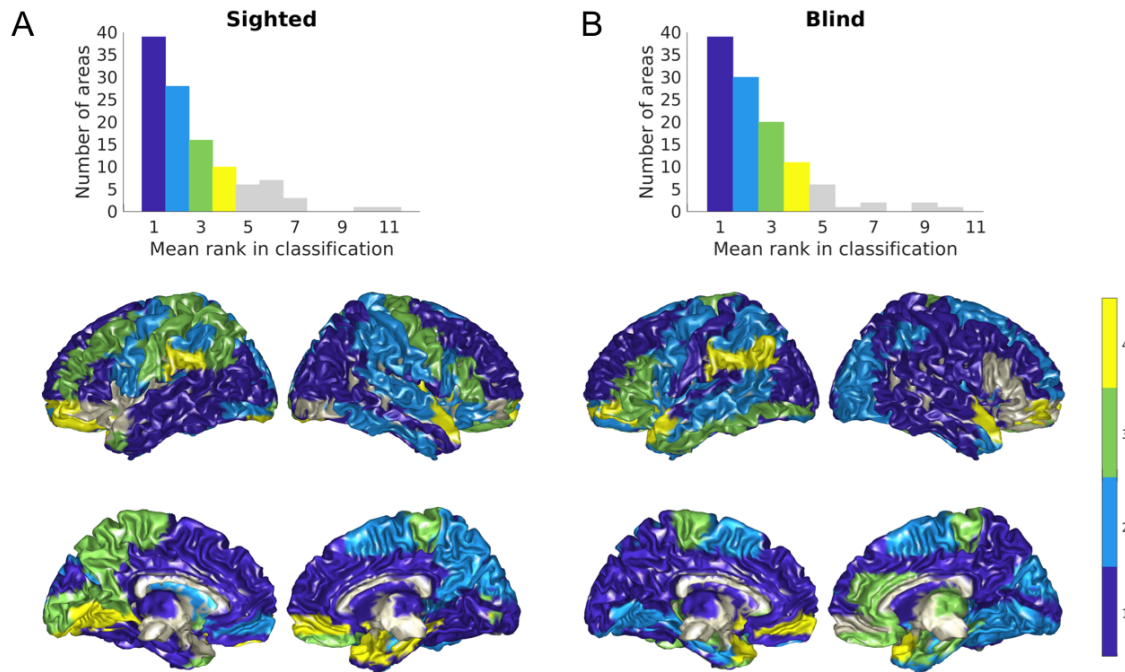

Fig 3. Classification results for the congenitally blind and the sighted with closed eyes. (A) Sighted eyes closed. (Upper) Histogram of mean ranks in classification across all 115 brain regions. (Lower) Topography of mean ranks (colors match ranks from histogram). (B) Congenitally blind. (Upper) Histogram of mean ranks in classification across all 115 brain regions. (Lower) Topography of mean ranks (colors match ranks from histogram). Bin width in is one for all subplots.

Spectral changes in sensory and right frontal regions in the congenitally blind

Based on the literature on intra- and cross-modal plasticity and behavioral adaptation in the CB, we hypothesized that spectral properties would change in congenital blindness. To test if (and which) brain areas differed in their spectral properties between the two groups, we implemented a cross-group classification drawing samples from the S-EC for the training and samples from the CB for the test group. Thus, region-specific single-subject spectra in the CB had to be identified based on the group-level clusters of the S-EC. This analysis resulted in a mean rank of 5.3 (range = 1.09 - 27.17).
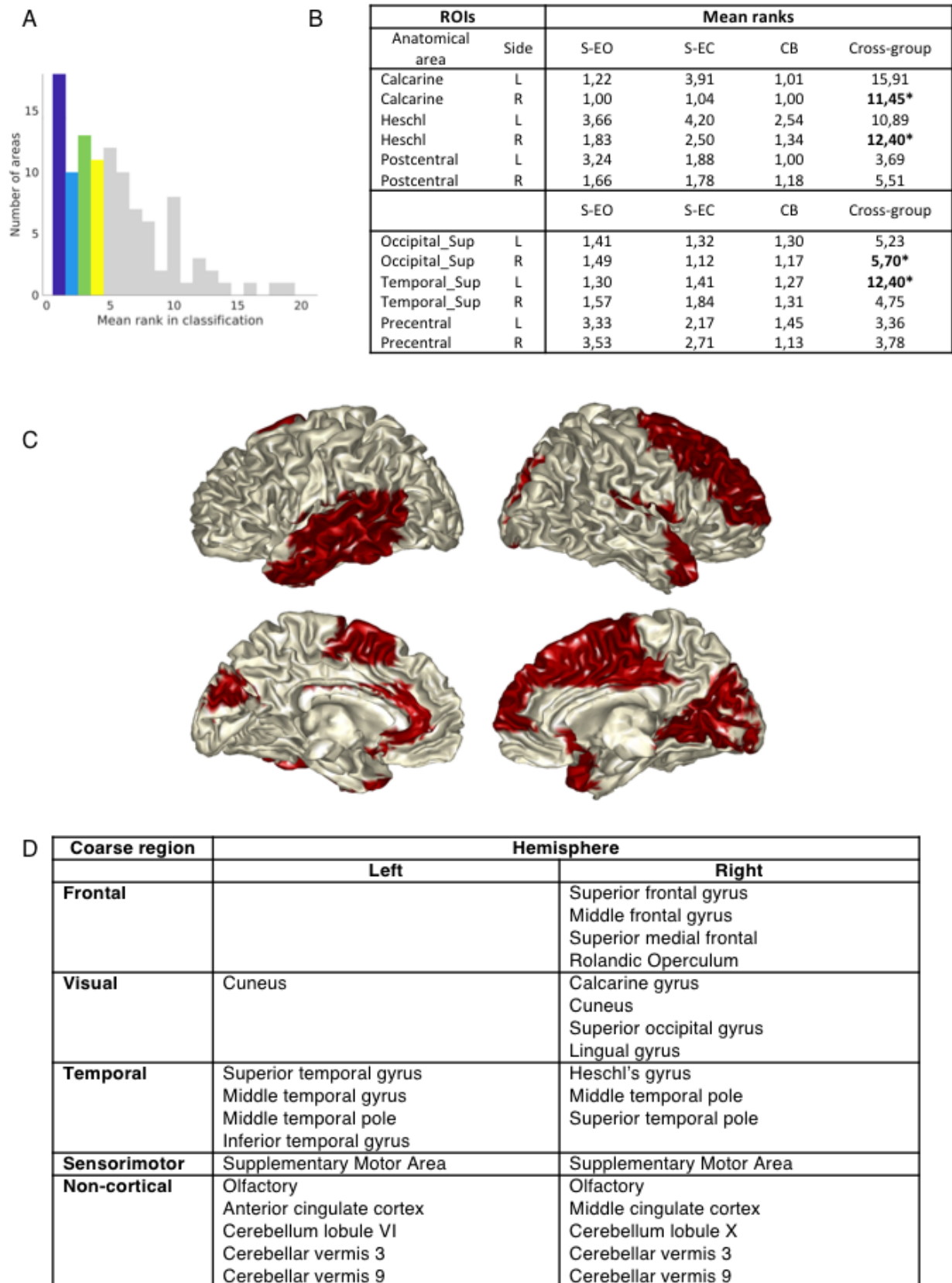
A

B

ROIs		Mean ranks			
Anatomical area	Side	S-EO	S-EC	CB	Cross-group
Calcarine	L	1,22	3,91	1,01	15,91
Calcarine	R	1,00	1,04	1,00	**11,45***
Heschl	L	3,66	4,20	2,54	10,89
Heschl	R	1,83	2,50	1,34	**12,40***
Postcentral	L	3,24	1,88	1,00	3,69
Postcentral	R	1,66	1,78	1,18	5,51
		S-EO	S-EC	CB	Cross-group
Occipital_Sup	L	1,41	1,32	1,30	5,23
Occipital_Sup	R	1,49	1,12	1,17	**5,70***
Temporal_Sup	L	1,30	1,41	1,27	**12,40***
Temporal_Sup	R	1,57	1,84	1,31	4,75
Precentral	L	3,33	2,17	1,45	3,36
Precentral	R	3,53	2,71	1,13	3,78

C

D

Coarse region	Hemisphere	
	Left	Right
Frontal		Superior frontal gyrus Middle frontal gyrus Superior medial frontal Rolandic Operculum
Visual	Cuneus	Calcarine gyrus Cuneus Superior occipital gyrus Lingual gyrus
Temporal	Superior temporal gyrus Middle temporal gyrus Middle temporal pole Inferior temporal gyrus	Heschl's gyrus Middle temporal pole Superior temporal pole
Sensorimotor	Supplementary Motor Area	Supplementary Motor Area
Non-cortical	Olfactory Anterior cingulate cortex Cerebellum lobule VI Cerebellar vermis 3 Cerebellar vermis 9	Olfactory Middle cingulate cortex Cerebellum lobule X Cerebellar vermis 3 Cerebellar vermis 9

Fig 4. Cross-group comparison. (A) Histogram of classification ranks. Bin width is one. (B) Table of mean classification ranks in primary and (extended) secondary sensory areas for the sighted (eyes open), sighted (eyes closed), congenitally blind participants and the cross-group classification. Asterisks indicate significantly different brain areas in the cross-group condition.

10

(C) Illustration of the topographic distribution of significantly different classification ranks in the cross-group condition (highlighted in red), as tested by a permutation procedure. (D) Table of all brain areas (out of 115) for which classification ranks were significantly different between congenitally blind and the sighted (eyes closed) (see C for significant areas highlighted in red).

For this condition, the distribution of mean ranks was broader compared to the within group conditions. 47.8% of 115 areas obtained classification ranks ranging from 1 to 4, while the automatic identification of the remaining regions was less precise (see Fig 4A). A visual inspection of mean ranks across areas and conditions (see Fig 4B) revealed that some brain regions (i.e., fusiform gyrus, left precentral gyrus) obtained similar rank values across conditions, while the rank value increased for other areas (i.e., Heschl's gyrus, calcarine).

Beyond these descriptive procedures, we inferentially tested for significantly different classification results in the cross-group condition compared to the control, i.e. classification within S-EC. In particular, this analysis assessed whether the mean rank of corresponding brain areas (e.g., calcarine-calcarine) between training (S-EC) and test (CB) sets differed from the classification ranks of the same region across all iterations (N=1000) in the control condition, thus accounting for the variability in the classification procedure. To this end, a distribution of ranks was generated from all iterations (N=1000) of the fitting procedure for the S-EC, against which the mean rank of the cross-group classification was tested; this was done separately for each ROI (see S2 Fig for the distributions of all brain areas). Fig 4C illustrates that cross-group classification ranks were significantly worse for several sensory as well as right frontal areas. This suggests that spectral profiles in sensory (e.g., right calcarine, right Heschl's gyrus, left superior temporal gyrus) and right frontal (e.g., right superior frontal gyrus) brain regions are different in the CB compared to the sighted (see Fig 4D for all ROIs showing significantly worse classification compared to the null-distribution).

Interestingly, the brain areas identified to have altered spectral profiles in the CB in the cross-group classification showed increased peak frequencies of the neuronal power in the group-level clusters (for a selection of brain areas with significant effects, see Fig 5A; spectra of all brain areas are shown in S1 Fig), in the auditory (more power in the alpha and beta band), and the right frontal areas (more power in the beta band). In

11

visual brain areas, power peaks were reduced in the alpha band, however, power increased in the low-gamma band. Post-hoc tests were performed to confirm these descriptive observations (Q = 0.05; FDR corrected p-value = .033; p-values < .033) (Fig 5B, frequencies where significant differences were observed are shaded in grey; see S3 Fig for all brain regions showing significantly worse cross-group classification). Note, however, that the differences in low-gamma power in calcarine between the CB and the S-EC were not significant in the post-hoc tests.
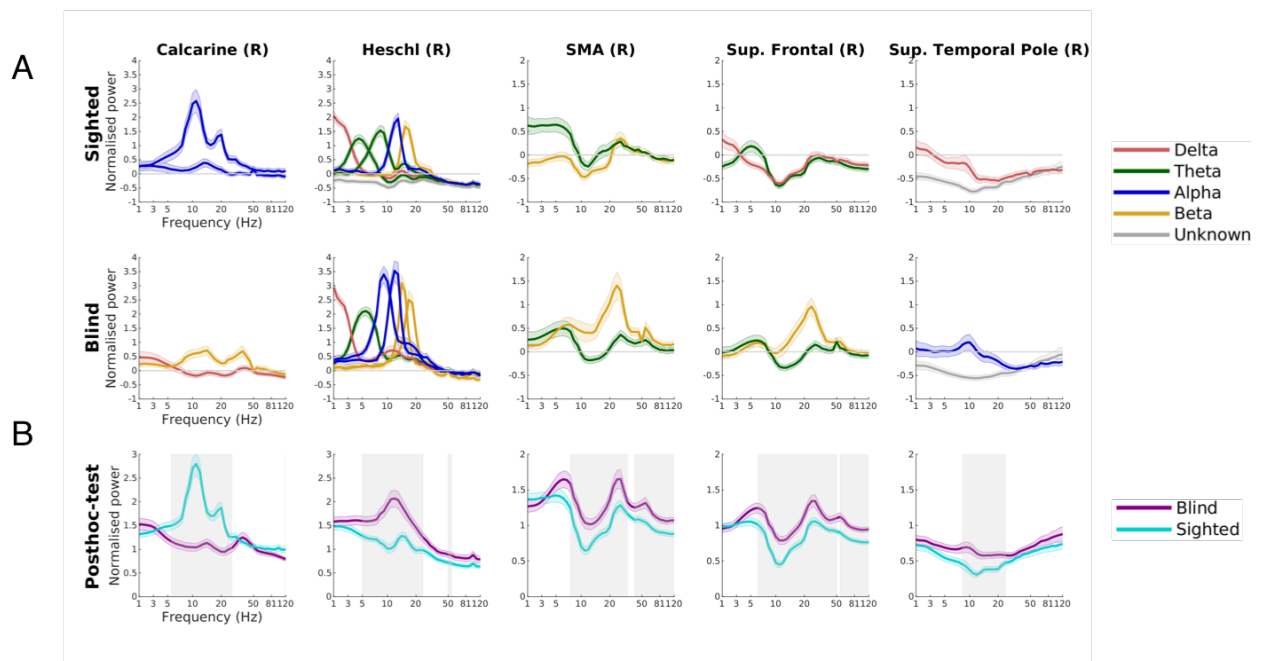
Fig 5. Comparison of sighted and blind spectral profiles. (A) A selection of the brain areas (columns) that showed significantly worse cross-group classification is displayed, separately for the S-EC and the CB (rows). Clusters are color-coded according to their peak frequency (legend on the right). (B) Post-hoc analysis of the spectral differences in a selection of significant brain regions (columns). Spectra represent normalized power spectra, averaged across trials and ROI voxels. Frequencies showing power differences between the groups (permutation test: Q=0.05; FDR corrected p-value= .033; p-values < .033) are illustrated as areas shaded in grey. The groups are color-coded (legend on the right).

Discussion

In this study we shed new light on visual deprivation-related changes in spectral properties across cortical brain areas and frequency bands. We implemented a novel whole-brain analysis pipeline, adapted from (40), capable of disclosing temporally-resolved spectral clusters specific to individual brain regions. K-means clustering and GMM were employed to establish spectral patterns across trials and subjects in the

three experimental groups (S-EO, S-EC, CB). A classifier automatically identified ana-tomical areas based on their spectral profiles for each group separately. Finally, a cross-group classification served to determine brain regions that were spectrally al-tered between the blind and the sighted. Our first main finding is that the clustering and classification procedures performed exceptionally well for all three groups (97-100% of areas were classified correctly in each group). This highlights consistent brain area-specific spectral properties across individuals within the sighted as well as the congen-itally blind groups. Crucially, second, we showed that visual deprivation gave rise to changes in the spectral profiles of especially sensory (auditory and visual) and right-frontal cortical areas, as indicated by significantly worse classification performance in the cross-group comparison for these brain areas, but not for other brain areas. More specifically, the spectral profiles of these areas in the CB, showed increased power in the alpha and/or beta frequency-bands in the right primary auditory cortex and right-frontal brain regions compared to the sighted. The visual cortex in the CB was charac-terized by a cluster with decreased alpha power compared to the sighted and a gamma (~40 Hz) peak, which was absent in the sighted. Our findings suggest that visual dep-rivation alters spectral properties particularly of certain brain areas, which have been previously suggested to show functional and structural reorganization. Neuronal power in these brain areas was altered in an area-specific manner, possibly reflecting changes in the functionally-specific processes in these areas (e.g., improved perfor-mance) in the congenitally blind.

Robust classification of brain areas based on spectral profiles

Spectral clustering and automatic classification revealed spectral profiles, classification ranks and distributions of classification ranks across cortex in the sighted (with eyes open) similar to the ones first reported by (40). The observed high classification ranks (Fig 2) suggest the correct brain areas were reliably assigned in the test data based on the spectral profiles of the corresponding area in the training data. Spectral profiles, for example of occipital regions, showed the typically observed peak at ~10 Hz. Spectral peaks in the beta-band (~20 Hz) were prominent across frontal and central brain areas, resembling previously reported natural frequencies of these brain areas (Fig 5;

(40,68,69)). While the spectral profiles of most brain areas well resembled those reported by Keitel and Gross, for some brain areas the spectral profiles differed (see S1 Fig). This suggests that the used recording system and/or the tested sample of participants can influence the specific profiles of some brain areas more than others. A test on a large dataset across different recording sites (i.e. several 100 recordings) will be necessary to clarify which spectral modes generalize across individuals in in the population. Importantly, within our sample, the spectral profiles were consistent across individuals (i.e. only group clusters were reported were at least ~70 % and on average ~97 % or ~94 % of participants contributed for the S-EO and S-EC, respectively). Thus, the present results show the robustness of brain area-specific spectral profiles, suggesting that (1) spectral profiles are characteristic properties of cortical regions and (2) show coherent patterns across subjects, which enables classification.

Crucially, a new finding of our study is that spectral clusters were also consistent within the group of congenitally blind individuals, as indicated by high classification performance (Fig 3B). Similar, as for the sighted group, brain regions could be identified reliably based on their spectral clusters suggesting spectral consistencies across individuals (i.e. only group clusters were reported were at least ~69 % and on average ~95 % of participants contributed). This result suggests, that adaptation of the cortex to visual deprivation leads to homogenously altered spectral fingerprints in congenitally blind individuals. The finding is in line with previous research, showing altered neuronal structures and activity in congenitally blind based on group-level analysis (27,70–72).

In our study deeper, sub-cortical, brain areas (in contrast to what has been reported by Keitel and Gross (40)) were not classified well (S1 Fig). A possible explanation is a lower SNR in deeper brain areas in our data compared to Keitel and Gross, due to the usage of different MEG systems.

Selective spectral plasticity across the brain

In the cross-group classification brain aeas of individual congenitally blind participants were classified based on the group-level spectral clusters of the sighted. In order to isolate visual deprivation-related effects, the sighted and congenitally blind participants were well matched in our study (cf. participants section). While in the cross-group classification, the classification for the majority of the brain areas was relatively good (i.e.,

14

low ranks; Fig 4A), spectra related to auditory, visual and right frontal regions were classified significantly worse compared to the within-sighted classification (Fig 4C; Note that overall ranks were higher, e.g. worse, in the cross-group classification compared to the within-group classifications). Importantly, these findings suggest that the spectral properties of brain areas are not homogenously altered by deprivation-related plasticity. Previously, a non-monotonic relationship between plasticity and stability across cortex, with decreases in plasticity from early visual to mid-level cortex and increases in plasticity higher in the visual cortical hierarchy, has been reported using fMRI (73, see also 74).

Spectral plasticity in sensory areas

Our findings highlight changes in spectral properties of auditory and visual cortex due to visual deprivation-related neuroplasticity. The findings are in line with previous reports, suggesting that cross-modal reorganization in visual cortex (15,24–28) and intra-modal reorganization in auditory cortex (31) affect neuronal activity in those sensory areas in blind individuals. Crucially, we show that these areas also show altered spectral characteristics.

Visual brain areas that were identified by the classifier to be spectrally different between the sighted and the blind involved primary visual cortex (calcarine sulcus) and its directly adjacent areas (cuneus, lingual gyrus), as well as more dorsal (SOG) visual regions and parts of the ventral visual stream (left ITG), involved in visual object recognition (75) (Fig 4D). In these areas, we observed a cluster with a clear visual alpha peak at 10 Hz for the sighted, and a second alpha cluster characterized by a smaller amplitude (Fig 5A). Keitel and Gross speculated that the second alpha cluster indicates continuous (present in ~80 % of the time) alpha suppression during visual fixation. However, our findings show that the second alpha cluster is similarly present during eyes open and eyes closed conditions (Fig 5A (upper), S1 Fig). In contrast, in the CB a first cluster with a strongly reduced alpha power peak, shifted towards higher (beta) frequencies, as well as a second cluster with an entirely absent alpha peak, was apparent in these visual areas (Fig 5A, B). This observation is in line with previous findings reporting a reduced or entirely absent alpha rhythm in the visual system in blind individuals (59–62). Interestingly, the spectral profile of one cluster in visual areas in

the blind included a peak in the low-gamma (~40 Hz) range which was entirely absent in the sighted (Note that this finding was not significant in the post-hoc tests, which tested effects independent from the clustering procedure; Fig 5B). This finding supports a recent report, which found enhanced gamma power correlations within visual cortex using MEG (62) in congenitally blind individuals. The alpha rhythm in humans likely reflects a local mechanism of rhythmic inhibition (76) mediating top-down control by feedback connections (77) and controlling gamma-amplitude (78, see 79). Synchronized gamma activity - controlled by alpha (de-)synchronization and phase - is suggested to serve a feedforward function, processing sensory information (77,80). In light of this, our results suggest that the decreased alpha and increased gamma power reflect an altered inhibitory/excitatory circuit in the visual system in congenital blindness (79,81). The reversed power patterns suggest that while visual cortex is functionally inhibited during rest and with closed eyes in the sighted, feedforward visual cortex processing seems to be enhanced in the congenitally blind, presumably due to disinhibition as consequence of atrophy in the thalamo-cortical connections, resulting in the reduced/absent alpha rhythm. This observation might also be related to studies reporting higher metabolism in the CB (82,83). A relevant question is, whether the altered spectral profile of visual cortex in congenitally blind individuals reflects changes in the functional role of visual cortex as reported during task-specific processing, i.e., an increased visual cortex recruitment during the processing of non-visual tasks (27,70,72,84).

Additionally, we found altered spectral profiles in auditory cortex with increases in the power in specific frequency bands. Brain areas in temporal cortex that were identified by the classifier to be spectrally different between the sighted and blind involved primary auditory cortex (right Heschl's gyrus), and areas of the ventral auditory stream (bilateral middle temporal pole, right superior temporal pole, left MTG, STG and ITG) (Fig 4D). In these areas, we observed increased power in higher frequencies (alpha to beta range) in the blind compared to the sighted (Fig 5A, B). Noticable, SMA similarly showed increased power in the beta-band (and absence of delta- and theta-band peaks) in the CB compared to the sighted (S1 Fig). Interestingly, previous research on ultra-fast speech processing in congenitally blind individuals reported that enhanced comprehension of ultra-fast speech in the blind is accompanied by increased speech-

16

tracking of higher frequencies in the alpha-beta range (16 Hz) in right auditory cortex (i.e., phase-alignment to the speech signal), compared to sighted individuals (19). An fMRI study suggested that pSTG, SMG, IFG, FG, V1 and the pulvinar might be involved in the tracking of ultra-fast speech in the blind (17). A large amount of studies connected temporal processing to the entrainment of auditory cortex oscillations (50,85–87). Thus, more generally, our findings of frequency increases of spectral power peaks might be related to increased temporal processing abilities, as often reported for congenitally blind individuals (6–8,12,15,18,19,88). In line with these assumptions, on the other side of the plasticity spectrum, age related decline in processing fast speech has been related to a slowing of theta-oscillations (89), additionally supporting the association of spectral dynamics within auditory cortex with temporal (speech) processesing. Further research is required to investigate the specifics of this effect.

Spectral plasticity in right frontal cortex

Beyond spectral reorganization in sensory cortices, our data suggest that particularly right-hemispheric frontal brain regions undergo neuroplastic adaptations as spectral clusters of right MFG and SFG were significantly different between the blind and the sighted. Previous research on plasticity, suggests that frontal cortex is particularly prone to plasticity related reorganization (73,74). Interestingly, changes in lateralization of cognitive processes have been reported previously in congenitally blind individuals. The predominance of the widely distributed frontotemporal language network in the left hemisphere is a robust finding, shown across different languages (90), developmental stages (91) and linguistic tasks (90,92,93). In congenital blindness, however, language processing likely is reflected in a reduced left-hemispheric lateralization of the frontotemporal network (94,95). Thus, it is possible that the altered spectral profiles in the right-hemispheric frontal brain regions observed here reflect changes in the hemispheric lateralization of the frontotemporal language network.

One limitation of this study is, that the interpretation of the changes of spectral clusters that were significantly different in the congenitally blind compared to the sighted is complicated by the multidimensionality of the spectral profiles. For that reason, we additionally performed a post-hoc analysis of the non-clustered data (based on the averaged brain area spectrum) to evaluate the cross-group differences between the sighted

17

and congenitally blind individuals (i.e., which frequencies show significant neuronal power differences; Fig 5B; results section). The analysis confirmed the findings from the spectral clustering approach, and highlighted the advantage of the clustering approach that was able to reveal the more fine grained pattern of brain area spectral peaks.

Concluding remarks

Our study supports the findings of robust brain area specific spectral profiles. Crucially, we provide novel findings that suggest consistently altered spectral profiles in congenitally blind compared to sighted individuals, particularly in visual and auditory brain areas, as well as right frontal cortex. Interestingly, overall spectral profiles in these brain areas showed increased power peaks in the blind. Depending on the brain area these altered spectral profiles are hypothesized to reflect changes in the excitatory-inhibitory cycle of visual cortex, or might be related (auditory and frontal brain areas) to the often enhanced auditory skills - such as enhanced speech processing - of congenitally blind indivdiuals.

Materials and Methods

Participants

The study was approved by the German Psychological Association (DGPs). All participants gave written informed consent prior to the experiments and received monetary compensation. The data were recorded in the context of a larger project (15,28). Three to four minutes of resting state MEG data were collected from a group of sighted and congenitally blind individuals matched in age and gender. During data collection the CB and the sighted (S-EC) were blindfolded, however, for the sighted an additional resting state measurement with open eyes was conducted (S-EO). The data reported here include 26 subjects for the CB (12 females; mean age: 37,8 years; SD: 10,2 years; age range: 22-55 years), 24 for the S-EC (11 females; mean age: 36,8 years; SD: 10,1 years; age range: 21-55 years) and 23 for the S-EO (11 females; mean age: 37,3 years; SD: 9,8 years; age range: 21-55 years). A few subjects needed to be excluded after

18

data collection because of corrupted resting state files (one subject for the CB, one subject for the S-EO) or no individual structural MRI scan (three subjects for the S-EC and S-EO). All participants were healthy with normal hearing (self-report) and assured no history of psychiatric or neurological disorders. One blind participant reported a history of depressive mood disorder, but was free of symptoms and without current treatment. Sighted participants had normal or corrected to normal vision (self-report). In the blind, vision loss was total and resulted from a variety of peripheral (pre)natal conditions (retinopathy of prematurity: n=9; genetic defect, n=5; congenital optic atrophy: n=2; Leber's congenital amaurosis: n=2; congenital cataracts, glaucoma: n= 2; congenital retinitis: n= 2; binocular anophthalmia: n= 2; retinitis pigmentosa: n= 1; congenital degeneration of the retina, n= 1). However, 17 participants reported minimal residual light perception.

MRI and MEG data acquisition

For all participants T1-weighted structural MRI scans were obtained with a 3T scanner (Siemens Magnetom Trio, Siemens, Erlangen, Germany). The MEG data were recorded in a magnetically shielded room using a 275-channel whole-head system (Omega, 2000, CTF Systems Inc.), while participants sat in an upright position. The data were acquired with a sampling rate of 1200 Hz. Prior to each experiment, the head position was measured relative to the MEG sensors and during the recording the head position was tracked.

Data analysis

The initial analyses in this study are adopted from of the analysis pipeline proposed by (40).The modifications of the analysis pipeline and the novel analysis will be stated in detail. All analyses were carried out using Matlab R2018a version (The Math Works Inc), the Fieldtrip Toolbox (version 20181104) and SPM12.

19

Data preparation in sensor space: preprocessing, artifact rejection, source localization

During preprocessing, the MEG signal was downsampled to 250Hz, denoised and detrended. To better capture the dynamically changing spectral properties of the brain, the continuous signal was segmented into trials of 0.8 s. Trials were declared as noisy and excluded when their z-score was higher than 2. On average, 7 trials were excluded, resulting in a mean of 340,3 trials (STD= 34,7) per subject (S-EO: mean = 346,7, STD = 37,4; S-EC: mean = 336,8, STD = 34,2; CB: mean = 338, STD 33,2). Due to shorter recordings in the present study, trial duration was slightly shortened relative to the Keitel & Gross (2016) (1 s) to increase statistical power. MEG channels were labeled as noisy and rejected when the ratio between their noise level (in STD) and that of the neighboring sensors (in STD) exceeded a value of 0.5 ((Sensor STD - Neighbor STD) / Neighbor STD; mean number of excluded channels = 1.22, STD = 1.34). Finally, using independent component analysis (ICA), data was cleaned from heartbeat, eye blinks and eye movements related artifacts (components were identified based on their time-course, topography and variance across trials). To prepare the source projection of the Fourier spectra, beamformer coefficients were obtained. For this purpose, we applied co-registration of individual T1-weighted MRI scans and the MEG coordinate system, realignment, segmentation and normalization to MNI space. A forward model was created using a single-shell model and LCMV beamformer coefficients (96) were calculated for the MEG time series for each individual voxel on the 10-mm regular grid.

Spectral analysis in sensor space

The analyses described in the following were performed for all three groups separately (CB, S-EO, S-EC). First, Fourier-spectra were calculated on 0.8 s long trials for each subject, using a multitaper approach (3 tapers) and zero-padding (length of 2 s). Second, using the previously computed LCMV coefficients, the complex Fourier spectra were projected into source space. Fourier spectra of individual voxels and segments were ratio normalized, i.e., divided by the mean power across all voxels and trials (see

S4 Fig for the power spectra used for the normalization in all groups). This ratio normalization resulted in voxel-specific spectral properties with values above/below one highlighting the differences of a given voxel to the mean spectral power across all voxels separately at each frequency. All values were subtracted by 1 (leading to values above/below zero), to facilitate the identification of changes in power (de/increases).

k-Means clustering and Gaussian mixture modelling of source-localized spectral activity

To identify region-specific spectral clusters in the individual subject, the brain was parcellated according to the AAL atlas (65) (116 anatomical areas). For one anatomical region (cerebellum 3L), however, interpolation between AAL atlas and source model was not successful. Thus, this region was excluded and all analyses are based on the remaining 115 anatomical areas. For each of the ROIs, voxels were grouped and power spectra were averaged across voxels. Clustering algorithms were employed to identify spectral clusters. First, trial-by-frequency matrices were subjected to a k-means algorithm (66). The algorithm established spectral clusters by finding coherent patterns across trials. Based on the silhouette criterion (97) across ROIs and subjects (we chose the highest value for optimal number of clusters) a predefined number of clusters was set (k = 9). Second, for each subject and ROI, GMMs (67) were fitted to the 9 clusters obtained from the k-means analysis (1st level GMM). The optimal number of clusters per brain region across all subjects were identified, evaluating first-level GMMs using the Silhouette criterion, and used for the group analysis. At the group level, k-means clustering was applied to the 1st level clusters in order to disclose consistent patterns across subjects. The optimal number of clusters per brain area, as assessed by the Silhouette criterion evaluation, was used as parameter for the algorithm. As before, k-means results were fed into GMM revealing the final clusters per brain region (2nd level GMM).

Automatic within group classification

A classifier was employed to test the specificity of region-specific spectral fingerprints. After splitting each group into half (training and test group), group-level clusters were calculated for the training group for all anatomical regions using k-means and GMM

clustering. For each brain region of the test group, the similarity of spectral profiles was assessed compared to all brain regions of the training group by computing the negative log-likelihood for all pairs of regions. This procedure, that is group assignment and classification, was repeated 1000 times (note that for the S-EO one subject was left out in every iteration to yield an even number of participants in training and test groups). On each iteration, an additional loop (N=100) controlled for interindividual noise by randomly drawing the adequate number of subjects (i.e., N_{S-EO}=11, N_{S-EC}=12, N_{CB}=13) from the test group with replacement, allowing a subject to enter multiple times or not at all. Put differently, while group assignment and number of subjects per group was kept constant for an iteration of the outer loop, the exact subjects from the group contributing to each inner iteration varied. Based on the mode of clusters identified per brain region in the 2nd level cluster analysis, the optimal number of clusters for the classification analysis was k=2. Likelihood values were ranked and averaged across iterations (20% trimmed mean). For further comparisons, only corresponding ROIs (e.g., how is the Heschl ROI in the test set ranked based on the training set Heschl ROI) were considered.

Additionally, to the descriptive report of the classification performance, here we tested whether a specific ROI (of the test set) was classified significantly better by the corresponding area of the training set, compared to all other 115 ROIs. This allowed us to exclude the possibility that classification performance was caused by unspecific effects – that is, generic fingerprints. To this end, each region's mean rank (averaged across iterations) was tested against a distribution of classification ranks generated from all other ROIs.

Automatic cross-group classification

Crucially, in order to identify differences in region-specific spectral properties between the CB and S-EC, we performed a cross-group classification. The same classification procedure was employed, however, the classifier was trained on one group (S-EC), while the other (CB) was utilized as the test set. As before, the classification procedure was repeated 1000 times, drawing a subset of N=12 per group on every iteration. Importantly, the randomization of subjects chosen on each iteration was identical to the one used for the within group classification in the S-EC (this is the reason why N=12,

22

instead of using all subjects of both groups). Thus, differences in the classification, as reflected by the ranks, could not be caused by the training set per se. In order to understand whether classification of brain regions was different in the cross-group condition, we tested the cross-group classification mean ranks against the distribution of ranks from the same ROI from the S-EC group. The distributions were generated by taking the classification rank of a corresponding area from training and test set (i.e. Calcarine) across all iterations (see S2 Fig for the distributions of all brain areas). We calculated the 95th percentile of the distribution and tested whether the cross-group mean rank of the current region fell above (significant) or below (not significant) this threshold.

To further assess the spectral profiles of brain areas that were significantly different in the cross-group classification, post-hoc permutation statistics were applied to the raw, normalized region-specific spectra (i.e., Fourier spectra without clustering procedure). The spectral analysis was calculated as in the main analysis (see above). For all significant brain regions seperately, power was averaged across voxels and segments, resulting in a single power value per frequency and per subject. Based on frequency by subject matrices for the CB and the S-EC, group differences in spectral power were assessed by randomly permuting (N=1000) the group assignment (CB vs. S-EC). To control for multiple comparisons, we used FDR (Q = 0.05).

Funding

References

1. Gougoux F, Lepore F, Lassonde M, Voss P, Zatorre RJ, Belin P. Pitch discrimination in the early blind. Nature. 2004;430(6997):309–309.

2. Lessard N, Paré M, Lepore F, Lassonde M. Early-blind human subjects localize sound sources better than sighted subjects. Nature. 1998;395(6699):278–80.

3. Gougoux F, Zatorre RJ, Lassonde M, Voss P, Lepore F. A functional neuroimaging study of sound localization: visual cortex activity predicts performance in early-blind individuals. Raichle M, editor. PLoS Biol. 2005;3(2):e27.

4. Bull R, Rathborn H, Clifford BR. The voice-recognition accuracy of blind listeners. Perception. 1983;12(2):223–6.

5. Foecker J, Best A, Hoelig C, Röder B. The superiority in voice processing of the blind arises from neural plasticity at sensory processing stages. Neuropsychologia. 2012;50(8):2056–67.

6. Röder B, Roesler F, Spence C. Early vision impairs tactile perception in the blind. Curr Biol. 2004;14(2):121–4.

7. Stevens AA, Weaver K. Auditory perceptual consolidation in early-onset blindness. Neuropsychologia. 2005;43(13):1901–10.

8. Hoetting K, Roesler F, Röder B. Altered auditory-tactile interactions in congenitllally blind humans: an event-related potential study. Exp Brain Res. 2004;159:370–81.

9. Röder B, Roesler F. Memory for environmental sounds in sighted, congenitally blind and late blind adults: evidence for cross-modal compensation. Int J Psychophysiol. 2003;50(1–2):27–39.

10. Röder B, Roesler F, Neville HJ. Auditory memory in congenitally blind adults: a behavioral-electrophysiological investigation. Cogn Brain Res. 2001;11(2):289–303.

11. Amedi A, Raz N, Pianka P, Malach R, Zohary E. Early 'visual' cortex activation correlates with superior verbal memory performance in the blind. Nat Neurosci. 2003;6(7):758–66.

12. Röder B, Kraemer UM, Lange K. Congenitally blind humans use different stimulus selection strategies in hearing: An ERP study of spatial and temporal attention. Restor Neurol Neurosci. 2007;25:12.

13. Lerens E, Araneda R, Renier L, De Volder AG. Improved beat asynchrony detection in early blind individuals. Perception. 2014;43(10):1083–96.

14. Carrara-Augustenborg C, Schultz BG. The implicit learning of metrical and non-metrical rhythms in blind and sighted adults. Psychol Res. 2019;83(5):907–23.

15. Rimmele JM, Gudi-Mindermann H, Nolte G, Röder B, Engel AK. Working memory training integrates visual cortex into beta-band networks in congenitally blind individuals. NeuroImage. 2019;194:259–71.

16. Hertrich I, Dietrich S, Moos A, Trouvain J, Ackermann H. Enhanced speech perception capabilities in a blind listener are associated with activation of fusiform gyrus and primary visual cortex. Neurocase. 2009;15(2):163–70.

17. Dietrich S, Hertrich I, Ackermann H. Ultra-fast speech comprehension in blind subjects engages primary visual cortex, fusiform gyrus, and pulvinar – a functional magnetic resonance imaging (fMRI) study. BMC Neurosci. 2013;14(1). Available from: https://bmcneurosci.biomedcentral.com/articles/10.1186/1471-2202-14-74

18. Trouvain J, Trouvain P-B. On the comprehension of extremely fast synthetic speech. Saarl Work Pap Linguist. 2007;9.

19. Hertrich I, Dietrich S, Ackermann H. Tracking the speech signal – Time-locked MEG signals during perception of ultra-fast and moderately fast speech in blind and in sighted listeners. Brain Lang. 2013;124(1):9–21.

20. Noppeney U, Friston KJ, Ashburner J, Frackowiak R, Price CJ. Early visual deprivation induces structural plasticity in gray and white matter. Curr Biol. 2005;15(13):R488–90.

21. Noppeney U. The effects of visual deprivation on functional and structural organization of the human brain. Neurosci Biobehav Rev. 2007;31(8):1169–80.

22. Jiang J, Zhu W, Shi F, Liu Y, Li J, Qin W, et al. Thick visual cortex in the early blind. J Neurosci. 2009;29(7):2205–11.

23. Park H-J, Lee JD, Kim EY, Park B, Oh M-K, Lee S, et al. Morphological alterations in the congenital blind based on the analysis of cortical thickness and surface area. NeuroImage. 2009;47(1):98–106.

24. Pascual-Leone A, Amedi A, Fregni F, Merabet LB. The plastic human brain cortex. Annu Rev Neurosci. 2005;28(1):377–401.

25. Burton H. Visual cortex activity in early and late blind people. J Neurosci. 2003;23(10):4005–11.

26. Bedny M, Pascual-Leone A, Dodell-Feder D, Fedorenko E, Saxe R. Language processing in the occipital cortex of congenitally blind adults. Proc Natl Acad Sci. 2011;108(11):4429–34.

27. Voss P, Zatorre RJ. Organization and reorganization of sensory-deprived cortex. Curr Biol. 2012;22(5):R168–73.

28. Gudi-Mindermann H, Rimmele JM, Nolte G, Bruns P, Engel AK, Röder B. Working memory training in congenitally blind individuals results in an integration of occipital cortex in functional networks. Behav Brain Res. 2018;348:31–41.

29. Elbert T, Sterr A, Rockstroh B, Pantev C, Müller MM, Taub E. Expansion of the tonotopic area in the auditory cortex of the blind. J Neurosci. 2002;22(22):9941–4.

30. Röder B, Roesler F, Hennighausen E, Nicker F. Event-related potentials during auditory and somatosensory discrimination in sighted and blind human subjects. Cogn Brain Res. 1996;4:17.

31. Röder B, Neville H. Developmental functional plasticity. Grafman J, Robertson I, editors. Handb Neuropsychol. 2003;(9):231–70.

32. Burton H, Snyder AZ, Raichle ME. Resting state functional connectivity in early blind humans. Front Syst Neurosci. 2014;8. Available from: http://journal.frontiersin.org/article/10.3389/fnsys.2014.00051/abstract

33. Pelland M, Orban P, Dansereau C, Lepore F, Bellec P, Collignon O. State-dependent modulation of functional connectivity in early blind individuals. NeuroImage. 2017;147:532–41.

34. Klinge C, Eippert F, Roder B, Buchel C. Corticocortical Connections Mediate Primary Visual Cortex Responses to Auditory Stimulation in the Blind. J Neurosci. 2010;30(38):12798–805.

35. Liu Y, Yu C, Liang M, Li J, Tian L, Zhou Y, et al. Whole brain functional connectivity in the early blind. Brain. 2007;130(8):2085–96.

36. Yu C, Liu Y, Li J, Zhou Y, Wang K, Tian L, et al. Altered functional connectivity of primary visual cortex in early blindness. Hum Brain Mapp. 2008;29(5):533–43.

37. Buzsaki G. Neuronal oscillations in cortical networks. Science. 2004;304(5679):1926–9.

38. Buzsáki G, Logothetis N, Singer W. Scaling brain size, keeping timing: evolutionary preservation of brain rhythms. Neuron. 2013;80(3):751–64.

39. Singer W. Neuronal oscillations: unavoidable and useful? Eur J Neurosci. 2018;48(7):2389–98.

40. Keitel A, Gross J. Individual human brain areas can be identified from their characteristic spectral activation fingerprints. Engel AK, editor. PLOS Biol. 2016;14(6):e1002498.

41. Giraud A-L, Kleinschmidt A, Poeppel D, Lund TE, Frackowiak RSJ, Laufs H. Endogenous cortical rhythms determine cerebral specialization for speech perception and production. Neuron. 2007;56(6):1127–34.

42. Engel AK, König P, Kreiter AK, Schillen TB, Singer W. Temporal coding in the visual cortex: new vistas on integration in the nervous system. Trends Neurosci. 1992;15(6):218–26.

43. Singer W. Cortical dynamics revisited. Trends Cogn Sci. 2013;17(12):616–26.

44. Raichle ME. The restless brain. Brain Connect. 2011;1(1):3–12.

45. Hipp JF, Engel AK, Siegel M. Oscillatory synchronization in large-scale cortical networks predicts perception. Neuron. 2011;69(2):387–96.

46. Singer W, Gray CM. Visual feature integration and the temporal correlation hypothesis. 1995;32.

47. Engel AK, Fries P, Singer W. Dynamic predictions: Oscillations and synchrony in top–down processing. Nat Rev Neurosci. 2001;2(10):704–16.

48. Lakatos P, Karmos G, Mehta AD, Ulbert I, Schroeder CE. Entrainment of neuronal oscillations as a mechanism of attentional selection. Science. 2008;320(5872):110–3.

49. Holcombe AO. Seeing slow and seeing fast: two limits on perception. Trends Cogn Sci. 2009;13(5):216–21.

50. Giraud A-L, Poeppel D. Cortical oscillations and speech processing: emerging computational principles and operations. Nat Neurosci. 2012;15(4):511–7.

51. VanRullen R. Perceptual rhythms. In: Wixted JT, editor. Stevens' Handbook of Experimental Psychology and Cognitive Neuroscience [Internet]. Hoboken, NJ, USA: John Wiley & Sons, Inc.; 2018 [cited 2019 Jul 29]. p. 1–44. Available from: http://doi.wiley.com/10.1002/9781119170174.epcn212

52. Portoles O, Borst JP, van Vugt MK. Characterizing synchrony patterns across cognitive task stages of associative recognition memory. Eur J Neurosci. 2018;48(8):2759–69.

53. Schroeder SCY, Ball F, Busch NA. The role of alpha oscillations in distractor inhibition during memory retention. Eur J Neurosci. 2018;48(7):2516–26.

54. Deco G, Jirsa VK, McIntosh AR. Emerging concepts for the dynamical organization of resting-state activity in the brain. Nat Rev Neurosci. 2011;12(1):43–56.

55. Raichle ME. The restless brain: how intrinsic activity organizes brain function. Philos Trans R Soc B Biol Sci. 2015;370(1668):20140172.

56. Engel AK, Gerloff C, Hilgetag CC, Nolte G. Intrinsic coupling modes: Multiscale interactions in ongoing brain activity. Neuron. 2013;80(4):867–86.

57. De Luca M, Beckmann CF, De Stefano N, Matthews PM, Smith SM. fMRI resting state networks define distinct modes of long-distance interactions in the human brain. NeuroImage. 2006;29(4):1359–67.

58. de Pasquale F, Della Penna S, Snyder AZ, Lewis C, Mantini D, Marzetti L, et al. Temporal dynamics of spontaneous MEG activity in brain networks. Proc Natl Acad Sci. 2010;107(13):6040–5.

59. Adrian ED. The Berger rhythm: potential changes from the occipital lobes in man. 1934;31.

60. Noebels JL, Roth WT, Kopell BS. Cortical slow potentials and the occipital EEG in congenital blindness. J Neurol Sci. 1978;37(1–2):51–8.

61. Kriegseis A, Hennighausen E, Roesler F, Röder B. Reduced EEG alpha activity over parieto-occipital brain areas in congenitally blind adults. Clin Neurophysiol. 2006;117(7):1560–73.

62. Hawellek DJ, Schepers IM, Röder B, Engel AK, Siegel M, Hipp JF. Altered intrinsic neuronal interactions in the visual cortex of the blind. J Neurosci. 2013;33(43):17072–80.

63. Schubert JTW, Buchholz VN, Foecker J, Engel AK, Röder B, Heed T. Oscillatory activity reflects differential use of spatial reference frames by sighted and blind individuals in tactile attention. NeuroImage. 2015;117:417–28.

64. Schepers IM, Hipp JF, Schneider TR, Röder B, Engel AK. Functionally specific oscillatory activity correlates between visual and auditory cortex in the blind. Brain. 2012;135(3):922–34.

65. Tzourio-Mazoyer N, Landeau B, Papathanassiou D, Crivello F, Etard O, Delcroix N, et al. Automated anatomical labeling of activations in SPM using a macroscopic anatomical parcellation of the MNI MRI single-subject brain. NeuroImage. 2002;15(1):273–89.

66. MacQueen J. Some methods for classification and analysis of multivariate observations. 1967;281–97.

67. Reynolds DA, Rose RC. Robust text-independent speaker identification using Gaussian mixture speaker models. IEEE Trans Speech Audio Process. 1995;3(1):72–83.

68. Rosanova M, Casali A, Bellina V, Resta F, Mariotti M, Massimini M. Natural Frequencies of Human Corticothalamic Circuits. J Neurosci. 2009;29(24):7679–85.

69. Ferrarelli F, Sarasso S, Guller Y, Riedner BA, Peterson MJ, Bellesi M, et al. Reduced natural oscillatory frequency of frontal thalamocortical circuits in schizophrenia. Arch Gen Psychiatry [Internet]. 2012 [cited 2019 Sep 22];69(8). Available from: http://archpsyc.jamanetwork.com/article.aspx?doi=10.1001/archgenpsychiatry.2012.147

70. Striem-Amit E, Ovadia-Caro S, Caramazza A, Margulies DS, Villringer A, Amedi A. Functional connectivity of visual cortex in the blind follows retinotopic organization principles. Brain. 2015;138(6):1679–95.

71. Magrou L, Barone P, Markov NT, Killackey HP, Giroud P, Berland M, et al. How areal specification shapes the local and interareal circuits in a macaque model of congenital blindness. Cereb Cortex. 2018;28(8):3017–34.

72. Voss P. Brain (re)organization following visual loss. Wiley Interdiscip Rev Cogn Sci. 2019;10(1):e1468.

73. Haak KV, Beckmann CF. Plasticity versus stability across the human cortical visual connectome. Nat Commun. 2019;10(1):3174.

74. Ortiz-Terán L, Diez I, Ortiz T, Perez DL, Aragón JI, Costumero V, et al. Brain circuit–gene expression relationships and neuroplasticity of multisensory cortices in blind children. Proc Natl Acad Sci. 2017;201619121.

75. Goodale MA, Milner AD. Separate visual pathways for perception and action. Trends Neurosci. 1992;15(1):20–5.

76. Haegens S, Nacher V, Luna R, Romo R, Jensen O. Alpha-Oscillations in the monkey sensorimotor network influence discrimination performance by rhythmical inhibition of neuronal spiking. Proc Natl Acad Sci. 2011;108(48):19377–82.

77. Michalareas G, Vezoli J, van Pelt S, Schoffelen J-M, Kennedy H, Fries P. Alpha-beta and gamma rhythms subserve feedback and feedforward influences among human visual cortical areas. Neuron. 2016;89(2):384–97.

78. Popov T, Kastner S, Jensen O. FEF-controlled alpha delay activity precedes stimulus-induced gamma-Band activity in visual cortex. J Neurosci. 2017;37(15):4117–27.

79. Röder B, Gudi-Mindermann H, Shareef I, Rimmele JM, Sourav S, Kekunnaya R, et al. Spectral profiles of resting state EEG in permanently congenital blind and sight recovery individuals. under revision.

80. van Kerkoerle T, Self MW, Dagnino B, Gariel-Mathis M-A, Poort J, van der Togt C, et al. Alpha and gamma oscillations characterize feedback and feedforward processing in monkey visual cortex. Proc Natl Acad Sci. 2014;111(40):14332–41.

81. Schmiedt JT, Maier A, Fries P, Saunders RC, Leopold DA, Schmid MC. Beta oscillation dynamics in extrastriate cortex after removal of primary visual cortex. J Neurosci. 2014;34(35):11857–64.

82. Veraart C, De Volder AG, Wanet-Defalque MC, Bol A, Michel C, Goffinet AM. Glucose utilization in human visual cortex is abnormally elevated in blindness of early onset but decreased in blindness of late onset. Brain Res. 1990;510(1):115–21.

83. Wanet-Defalque M-C, Veraart C, De Volder A, Metz R, Michel C, Dooms G, et al. High metabolic activity in the visual cortex of early blind human subjects. Brain Res. 1988;446(2):369–73.

84. Bedny M. Evidence from blindness for a cognitively pluripotent cortex. Trends Cogn Sci. 2017;21(9):637–48.

85. Gross J, Hoogenboom N, Thut G, Schyns P, Panzeri S, Belin P, et al. Speech rhythms and multiplexed oscillatory sensory coding in the human brain. Poeppel D, editor. PLoS Biol. 2013;11(12):e1001752.

86. Rimmele JM, Gross J, Molholm S, Keitel A. Editorial: Brain oscillations in human communication. Front Hum Neurosci [Internet]. 2018 [cited 2019 Jan 16];12. Available from: http://journal.frontiersin.org/article/10.3389/fnhum.2018.00039/full

87. Rimmele JM, Morillon B, Poeppel D, Arnal LH. Proactive sensing of periodic and aperiodic auditory patterns. Trends Cogn Sci. 2018;22(10):870–82.

88. Dietrich S, Hertrich I, Ackermann H. Training of ultra-fast speech comprehension induces functional reorganization of the central-visual system in late-blind humans. Front Hum Neurosci [Internet]. 2013 [cited 2019 Feb 22];7. Available from: http://journal.frontiersin.org/article/10.3389/fnhum.2013.00701/abstract

89. Penn LR, Ayasse ND, Wingfield A, Ghitza O. The possible role of brain rhythms in perceiving fast speech: Evidence from adult aging. J Acoust Soc Am. 2018;144(4):2088–94.

90. Binder JR, Desai RH, Graves WW, Conant LL. Where is the semantic system? A critical review and meta-analysis of 120 functional neuroimaging studies. Cereb Cortex. 2009;19(12):2767–96.

91. Dehaene-Lambertz G, Montavont A, Jobert A, Allirol L, Dubois J, Hertz-Pannier L, et al. Language or music, mother or Mozart? Structural and environmental influences on infants' language networks. Brain Lang. 2010;114(2):53–65.

92. Vigneau M, Beaucousin V, Hervé PY, Duffau H, Crivello F, Houdé O, et al. Meta-analyzing left hemisphere language areas: Phonology, semantics, and sentence processing. NeuroImage. 2006;30(4):1414–32.

93. Friederici AD. Towards a neural basis of auditory sentence processing. Trends Cogn Sci. 2002;6(2):78–84.

94. Roeder B, Stock O, Bien S, Neville H, Roesler F. Speech processing activates visual cortex in congenitally blind humans: Plasticity of language functions in blind adults. Eur J Neurosci. 2002;16(5):930–6.

95. Lane C, Kanjlia S, Richardson H, Fulton A, Omaki A, Bedny M. Reduced left lateralization of language in congenitally blind individuals. J Cogn Neurosci. 2017;29(1):65–78.

96. Van Veen BD, Van Drongelen W, Yuchtman M, Suzuki A. Localization of brain electrical activity via linearly constrained minimum variance spatial filtering. IEEE Trans Biomed Eng. 1997;44(9):867–80.

97. Rousseeuw PJ. Silhouettes: A graphical aid to the interpretation and validation of cluster analysis. J Comput Appl Math. 1987;20:53–65.